Supplementary Figure Legends

Supplementary Figure 1.

a) Interaction of FLAG-tagged YAP with endogenous BRD4, BRD2 and TEAD1 in HEK293T nuclear extracts. Each co-IP experiment was performed three times with similar results.
b) Schematic representation of the TAZ constructs here used, and Western blot of recombinant BRD4 pulled-down by the indicated GST-TAZ constructs. Similar results were obtained in two additional independent experiments. TB: TEAD binding domain; TA: Transcriptional Activation domain; WW: WW protein domain.
c) GST pulldown assay with the indicated GST-TAZ constructs and nuclear extracts of HEK293T expressing FLAG-BRD4. All TAZ constructs retain the ability to interact with TEAD1. The experiment was performed three times with similar results.
d) Recombinant BRD4 is pulled-down by GST-TAZ even after deletion of the WW domain (ΔWW). One of three independent experiments (all generating similar results) is shown.
e) *YAP1* and *WWTR1* (*TAZ*) were efficiently downregulated by YAP/TAZ siRNAs in replicate samples (n=2 independent samples per each experimental condition) used for RNA-seq. Individual samples are shown.
f) Genes activated by YAP/TAZ are defined as genes significantly downregulated by both the combinations of YAP/TAZ siRNAs used in this study.
g) Box-and-whiskers plots of expression values of YAP/TAZ direct targets (n=616) vs. genes not activated by YAP/TAZ (not YT targets, n=771) in MDA-MB-231 cells. The box includes values within the 25^{th} and 75^{th} percentile (with the median highlighted by the line in the middle) and whiskers extend from the 10^{th} to the 90^{th} percentile. The group of not YT targets represents genes not significantly affected by YAP/TAZ depletion (FDR>0.05) in our RNA-seq dataset. **** $p<10^{-10}$ (one-tailed Mann-Whitney U test).
h) Box-and-whiskers plots (defined as in g) of expression values of genes expressed in MDA-MB-231 cells, classified according to biological function and activation by YAP/TAZ. *** $p<10^{-7}$; **** $p<10^{-10}$ (one-tailed Mann-Whitney U test) (n= 8650, 908, 541, respectively).
i) The fraction of genes directly activated by YAP/TAZ, which are negatively regulated by JQ1, is larger than the fraction of all expressed genes downregulated by the same treatment.
j) Left: genes inhibited by JQ1 (n=2832) were stratified in four groups, according to the level of downregulation (cut-off: FC = -1.5, -1.8, -2.5; all groups contain a comparable number of genes);

YAP/TAZ regulated genes are more represented among the most downregulated genes. Right: upon treatment with JQ1 (1μM, 24h), downregulation is more effective for genes that are also YAP/TAZ targets (n=1451); data are presented as in g. **** $p<10^{-10}$ (one-tailed Mann-Whitney U test)

k) Box-and-whiskers plots showing fold change in expression of genes related to cell proliferation, comparing the effect of JQ1 (1μM, 24h) on all YAP/TAZ targets (n=541) vs. not-YAP/TAZ targets (n=908); data are presented as in g. **** $p<10^{-10}$ (one-tailed Mann-Whitney U test)

l) RT-qPCR for representative YAP/TAZ activated genes showing downregulation upon treatment with BET inhibitors (1μM, 24h). The experiment was repeated three times with similar results.

m) RT-qPCR for YAP/TAZ target genes, showing downregulation upon depletion of BRD4 alone (siBRD4) or BRD2/3/4 (siBRD mix A and B). Data are presented as individual data points (n=2 independent samples) + average (bar). The experiment was repeated three times with similar results.

n) Representative confocal images for YAP/TAZ IF staining in MDA-MB-231 cells upon treatment with BET inhibitors (1μM, 24h). Scale bar is 20 μm. IF was performed three times with similar results.

o) Fraction of genes downregulated by the indicated drugs in MDA-MB-231 cells (genes activated by YT, n=2073; all expressed genes, n=10101).

Supplementary Figure 2.

a) ChIP-qPCR showing the specificity of anti-BRD4 antibody. ChIP with pre-immune IgG displayed background signal. DNA enrichment was calculated as fraction of input.

b) Box-and-whiskers plots showing the distribution of BRD4 ChIP-seq signal (expressed as normalized read density, RPKM) on promoters and enhancers in MDA-MB-231 cells. The box includes values within the 25^{th} and 75^{th} percentile (with the median highlighted by the line in the middle) and whiskers extend from the 5^{th} to the 95^{th} percentile. H3K27ac classes were arbitrarily defined. (inactive promoters, n=4618; active promoters, n=10376; poised enhancers, n=62618; active enhancers, n=26228+7429+3772)

c) Box-and-whiskers plots (defined as in b) showing the change in BRD4 genomic occupancy in JQ1-treated (left) or YAP/TAZ-depleted cells (right) vs. control cells (DMSO), comparing enhancers with (n=5169) or without YAP/TAZ peaks (n=30281). **** $p<10^{-10}$ (one-tailed Mann-Whitney U test)

d) Heatmap showing BRD4 binding on enhancers containing YAP/TAZ peaks in MDA-MB-231 cells, in a window of ±1kb centered on the summit of YAP/TAZ peaks.

e) Validation by ChIP-qPCR of BRD4 detachment from enhancers containing YAP/TAZ peaks upon treatment with JQ1 or YAP/TAZ depletion. ChIP with pre-immune IgG displayed only background signal and is shown for control cells only. DNA enrichment was calculated as fraction of input and is presented as % of BRD4 binding in control cells (DMSO).

f) BRD4 binding (expressed as reads per million of mapped reads, RPM) across all active enhancers in MDA-MB-231 cells. Enhancers surpassing the inflection point are defined as superenhancers. Some YAP/TAZ-occupied typical enhancers and superenhancers are indicated by orange and red dots, respectively, and are named according to their associated genes.

g) 80% of superenhancers contain YAP/TAZ peaks.

h) Box-and-whiskers plots showing Log_2 fold change in expression level upon treatment with JQ1 of genes regulated by typical enhancers without YAP/TAZ peaks (n=2925 genes), with YAP/TAZ peaks (n=1543 genes) and superenhancers (n=781 genes). The box includes values within the 25th and 75th percentile (with the median highlighted by the line in the middle) and whiskers extend from the 10th to the 90th percentile. *** p=0.00015; ns: p=0.3 (one-tailed Mann-Whitney U test).

i) GST-YAP interacts with FLAG-BRD4 (in nuclear extracts of HEK293T cells) even in the presence of JQ1 or upon mutation of BRD4 bromodomains. Similar results were obtained with GST-TAZ

(data not shown). The experiment was repeated three times with similar results. WT=wild type; BD=BD-mutant.

j) ChIP-qPCR verifying reduction of BRD4 binding at promoters of YAP/TAZ target genes in JQ1-treated and YAP/TAZ-depleted MDA-MB-231 cells. Data are presented as in e. Similar results were obtained in two independent ChIP-qPCR experiments and by ChIP-seq.

Supplementary Figure 3.

a) ChIP-qPCR showing that YAP and TAZ binding at enhancers is not affected by JQ1 in MDA-MB-231 cells. ChIP with pre-immune IgG displayed only background signal. DNA enrichment was calculated as fraction of input and is presented as % of YAP or TAZ binding in control cells (DMSO). Data are presented as individual data points (n=2 independent samples) + average (bar). Two additional experiments with similar results were performed.

b) RT-qPCR showing that sustained expression of wild-type YAP does not rescue the expression of YAP/TAZ target genes in MDA-MB-231 cells depleted of BET proteins or treated with BET inhibitors (1μM, 24h). Exogenous YAP, instead, can rescue the expression of the same genes after YAP/TAZ depletion. Data are presented as individual data points (n=2 independent samples) + average (bar). The experiment was performed twice with similar results.

c) RT-qPCR showing that sustained expression of human BRD4 does not rescue the expression of YAP/TAZ target genes in MDA-MB-231 cells upon depletion of YAP/TAZ. Exogenous BRD4, instead, can rescue the expression of the same genes after depletion of endogenous BRD4. Data are presented as individual data points (n=2 independent samples) + average (bar). Similar results were obtained in two independent experiments

d) ChIP-qPCR verifying YAP binding at enhancers of YAP/TAZ target genes in YAP5SA-overexpressing MCF10A cells. DNA enrichment was calculated as fraction of input and is presented as fold vs. control cells.

e) Western blot showing overexpression of YAP5SA in MCF10A cells, with or without JQ1 (1μM, 24h). The experiment was performed twice with similar results.

f) Depletion of LATS1/2 in MCF10A cells induces the activation of endogenous YAP/TAZ. Treatment with JQ1 (1μM, 24h) impairs YAP/TAZ-dependent gene responses in LATS1/2-depleted cells (siLATS, 72h). Gene expression levels were determined by RT-qPCR; data are presented as individual data points (n=2 independent samples) + average (bar). The experiment was performed twice with similar results.

Supplementary Figure 4.

a) Box-and-whiskers plots showing the change in RNA-Pol II genomic occupancy in YAP/TAZ-depleted cells vs. control cells (DMSO), comparing promoters of genes not activated by YAP/TAZ (n=8026) with promoters of YAP/TAZ target genes (n=616). Each box includes values within the 25^{th} and 75^{th} percentile (with the median highlighted by the line in the middle) and whiskers extend from the 5^{th} to the 95^{th} percentile. **** $p<10^{-10}$ (one-tailed Mann-Whitney U test)

b) Average RNA-Pol II ChIP-seq profile on the promoters of YAP/TAZ target genes (n=616) in MDA-MB-231 cells, in a window of ±1.5 kb centered on TSS.

c) ChIP-qPCR verifying RNA-Pol II binding to promoters of established YAP/TAZ targets in MDA-MB-231 cells treated with DMSO or JQ1 (1μM, 24h), or transfected with YAP/TAZ siRNAs (48h). GAPDH promoter represents a non-YAP/TAZ target. ChIP with pre-immune IgG displayed background signal (which was comparable in all samples). DNA enrichment was calculated as fraction of input and is presented as % of RNA-Pol II binding in control cells (DMSO).

d) Western blot showing RNA-PolII in immunocomplexes of endogenous YAP in MDA-MB-231 nuclear extracts. The interaction is lost upon depletion of BRD4. The experiment was performed three times with similar results.

e) Genome browser view of RNA-Pol II binding profiles at representative promoters of YAP/TAZ target genes.

f) RT-qPCR showing that sustained expression of mouse BRD4 deficient in HAT activity (ΔHAT) does not rescue the expression of YAP/TAZ target genes in MDA-MB-231 cells depleted of endogenous BRD4 (siBRD4). Exogenous wild-type mouse BRD4 (WT), instead, can rescue the expression of the same genes. Data are presented as individual data points (n=2 independent samples) + average (bar). Similar results were obtained in two independent experiments.

g) Linear correlation between BRD4 occupancy and H3K122ac levels (both expressed in RPKM) on the TSS of YAP/TAZ target genes (n=616). r^2 was calculated using linear regression analysis (F-test p-value <0.0001).

h) ChIP-qPCR verifying H3K122ac levels on the promoters of established YAP/TAZ targets in MDA-MB-231 cells treated with DMSO or JQ1 (1μM, 24h), or transfected with YAP/TAZ siRNAs (48h). Data are presented as in c. Similar results were obtained in two independent ChIP-qPCR experiments and by ChIP-seq.

Supplementary Figure 5.

a) Western blot showing effective downregulation of BRD4 by shRNAs, and sustained expression of exogenous YAP in MCF10A+YAP5SA cells. GAPDH serves as loading control. Similar results were obtained in three independent experiments.
b) Left: quantification of colonies formed by MDA-MB-231 cells in soft agar assays. Assays were performed in the presence of doxycycline to induce the expression of control or BRD4 shRNAs. Data are presented as individual data points (n=3 independent samples) + average (bar). Right: western blot showing that BRD4 shRNAs downregulate BRD4 protein levels, without affecting YAP or TAZ. GAPDH serves as loading control. Similar results were obtained in three independent experiments.
c) Quantification of colonies formed by MDA-MB-231 cells in soft agar assays, upon treatment with 0.1μM or 1μM JQ1 for the entire experiment. as individual data points (n=3 independent samples) + average (bar). Similar results were obtained in three independent experiments.
d) Representative H&E staining of sections of mammary glands from *MMTV-Cre;Apc$^{fl/fl}$* mice. Scale bar is 0.1mm. The same phenotype was observed in n=4 mice.
e) Representative immunofluorescence (IF) pictures of mammary glands from *MMTV-Cre;Apc$^{fl/fl}$* mice, showing discontinuities in the layer of K14-positive cells in hyperplastic ducts. Scale bar is 50 μm. IF staining was performed in sections from n=4 mice, with similar phenotypes.
f) Representative HE staining of sections of mammary glands from *MMTV-Cre;Apc$^{fl/fl}$* mice, treated with vehicle (n=5) or BAY-BET inhibitor (n=5) for 6 weeks. Scale bar is 0.1mm.
g) Representative H&E staining of sections of mammary glands from *Apc$^{fl/fl}$* mice, treated with BAY-BET inhibitor, showing that mammary ducts maintain a normal morphology. Scale bar is 0.1mm. The same phenotype was observed in n=3 mice.
h) Representative immunofluorescence (IF) pictures of mammary glands from *Apc$^{fl/fl}$* mice treated with BAY-BET inhibitor, showing normal distribution of K8 and K14 in the mammary ducts. Scale bar is 25 μm. IF staining was performed in sections from n=3 mice, with similar phenotypes.

Supplementary Figure 6.

a) Representative IF showing that Albumin-Cre^{ERT2} drives the excision of the LSL cassette upstream of the YFP reporter specifically in hepatocytes (HNF4α+). Biliary epithelial cells (KRT19+) remain YFP-negative. PV=portal vein; D=bile duct. Scale bar is 50 μm.

b) Western blot showing the expression of YAPS127A in liver extracts from *Albumin-Cre^{ERT2}; R26-LSL-rtTA; tet-O-YAPS127A* (+YAP^{HEP}) mice. All mice received tamoxifen to activate *Cre* and rtTA expression, and then doxycycline to induce the expression of YAPS127A; treatment with BAY-BET-inhibitor does not impair YAPS127A expression. Two mice per experimental condition are shown; YAP levels were verified in all mice included in experimental groups, with results similar to those shown here.

c) Quantification of SOX9/HNF4α double positive cells, presented as % of all HNF4α positive cells. Dots represent portal areas captured across stained liver sections of 3 control mice treated with vehicle (n=6), 3 control mice treated with BAY-BET-inhibitor (n=6), 5 +YAP^{HEP} mice treated with vehicle (n=18), and 4 +YAP^{HEP} mice treated with BAY-BET-inhibitor (n=14); mean and SD are shown. See a representative image in Figure 6a.

d) RT-qPCR showing *Sox9* regulation in mouse liver by transgenic YAP overexpression (+YAP^{HEP}) and treatment with BET inhibitor. Each dot represents a mouse (control mice + vehicle, n=4; control mice + BAY-BET-inh, n=4; +YAP^{HEP} mice + vehicle, n=7; +YAP^{HEP} mice + BAY-BET-inh, n=9); mean and SD are shown. *** p=0.00025, unpaired t test, two-tailed

e) RT-qPCR showing *Spp1* regulation in mouse liver by transgenic YAP overexpression (+YAP^{HEP}) and treatment with BET inhibitor. Data are presented as in d. **** p=0.000001, unpaired t test, two-tailed

f) Representative hematoxylin and eosin (H&E) staining of liver sections from the indicated mice. Scale bars are 100μm. n=4 mice for both groups.

g) Representative SOX9/HNF4α IF picture of liver from control mice, treated with BAY-BET inhibitor (n=4 mice, all showing the same phenotype). Scale bar is 50μm.

h) Immunohistochemistry of Ki67 in liver sections from the indicated mice. Scale bar is 100μm. Ki67 staining was performed in at least three additional mice for each experimental condition, with similar results.

i) Quantification of acinar-to-ductal metaplasia (ADM) events in pancreatic acinar 3D culture in the presence of doxycycline. Treatment with JQ1 opposes YAP-induced ADM in organoids. Data are presented as individual data points (n=2 cultures) + average (bar). The experiment was repeated four times with similar results.

j) RT-qPCR of pancreatic acinar 3D cultures. Expression values are normalized to 18S rRNA. Data are presented as individual data points (n=2 cultures) + average (bar). The experiment was repeated four times with similar results.

k) Percentage viability of parental SKMEL28 transduced with EGFP or YAP5SA, treated with 3 μM vemurafenib with or without JQ1(1μM). Data are normalized to DMSO-treated cells and are presented as data points (n=8 samples, independently treated and evaluated) + mean (bar). Three independent experiments were performed with similar results.

l) RT-qPCR for YAP/TAZ target genes showing upregulation upon YAP5SA overexpression in SKMEL28 cells and downregulation upon treatment with BET inhibitors (1μM, 24h) or depletion of BRD2/3/4 (siBRD mix A and B). Data are presented as individual data points (n=2 independent samples) + average (bar). The experiment was repeated twice with similar results.

m) TEAD luciferase reporter assay (8xGTIIC-lux) in M229 and M229-R5 melanoma cells. JQ1 doses ranged from 1nM to 1μM. Data are normalized to parental M229 cells and are presented as individual data points (n=2 independent samples) + average (bar). The experiment was repeated twice with similar results.

n) Viability curves of parental SKMEL28 and vemurafenib-resistant SKMEL28 cells, or parental M229 and vemurafenib-resistant M229 cells, treated with increasing doses of vemurafenib (1nM to 10μM) with or without JQ1(1μM). The green line shows the effect of JQ1 alone (1μM). Data are presented as in k. The experiment was performed three times with similar results.

o) Cell viability assay of vemurafenib-resistant SKMEL28 (R2) and vemurafenib-resistant M229 (R5) cells, transfected with the indicated siRNAs and treated with DMSO or 3μM vemurafenib. Data are presented as in k. The experiment was performed three times with similar results.

p) Analyses of a dataset of human hepatocellular carcinomas with signatures of shared YAP/TAZ/BET targets vs. BET targets that were not YAP/TAZ targets, identified from analyses of YAP/TAZ-depleted or JQ1-treated HepG2 cells. Only common YAP/TAZ/BET targets can predict survival (Log-rank Mantel Cox Test).

q) Box plots showing time to disease progression in a cohort of patients with BRAF-mutant melanoma stratified according to the indicated signatures. Only common YAP/TAZ/BET targets have predictive capacity (unpaired t-test with Welch's correction).

Supplementary Figure 7.

Uncropped versions of the Western blots used in this manuscript.

SUPPLEMENTARY FIGURE 1

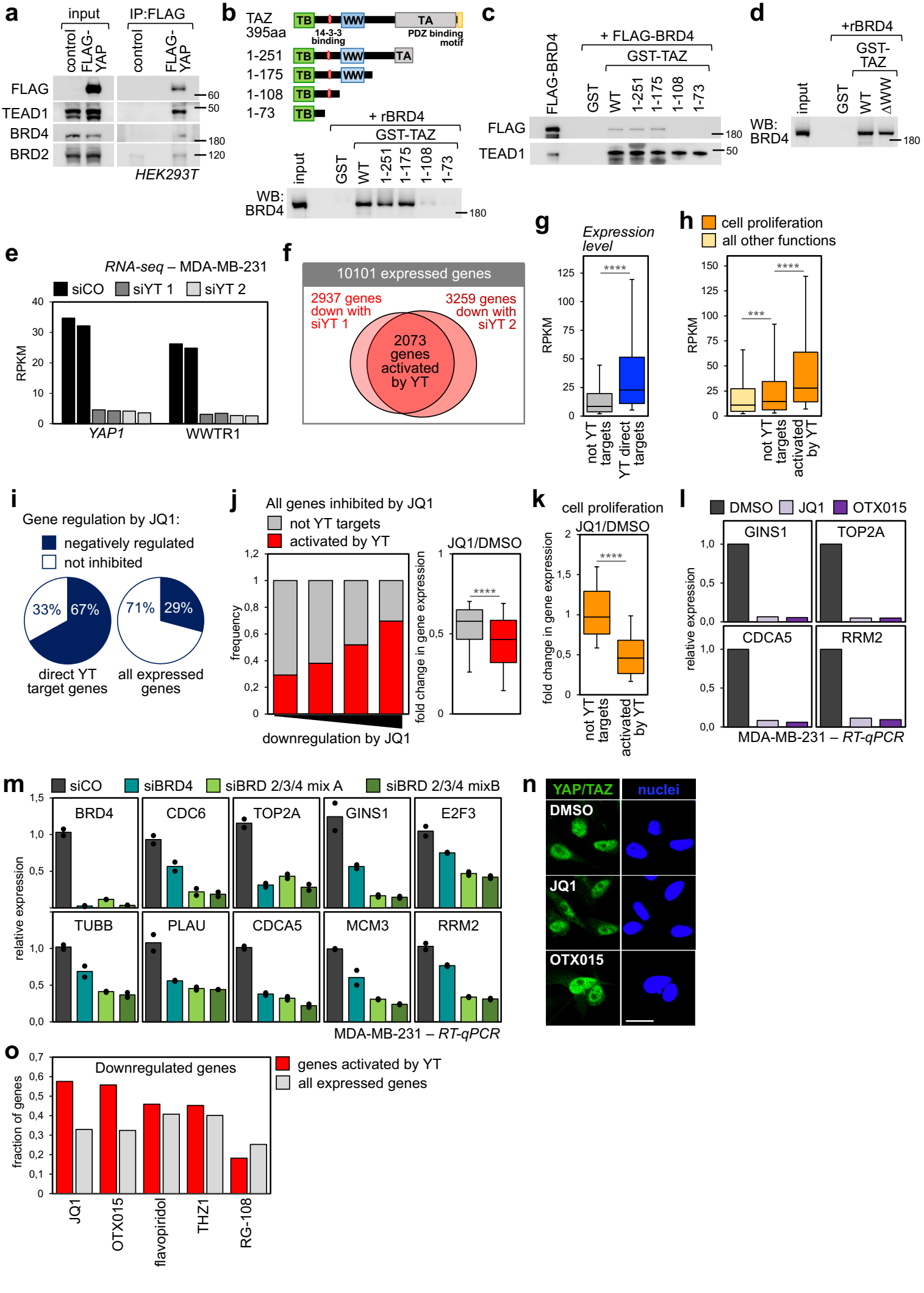

SUPPLEMENTARY FIGURE 2

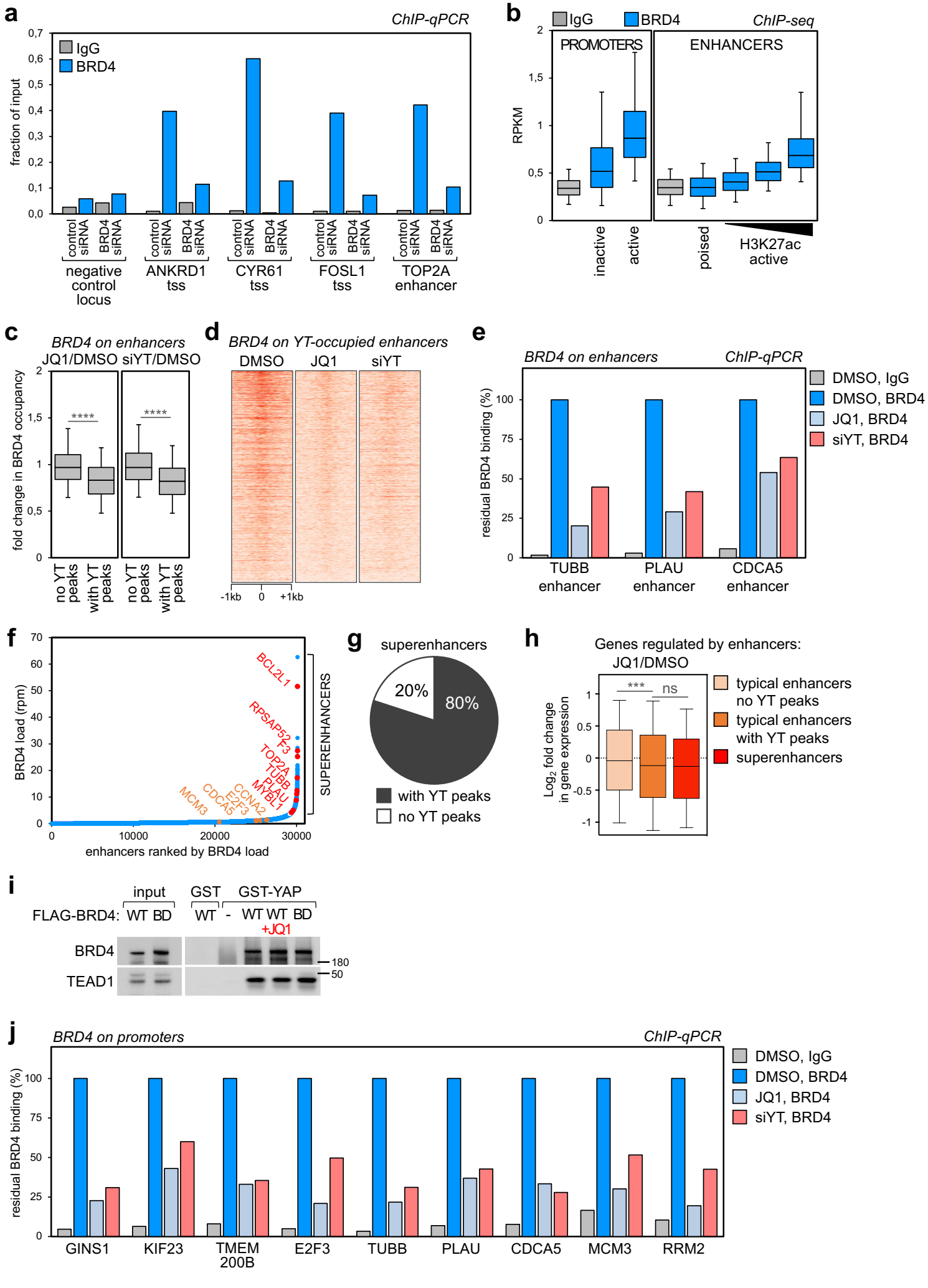

SUPPLEMENTARY FIGURE 3

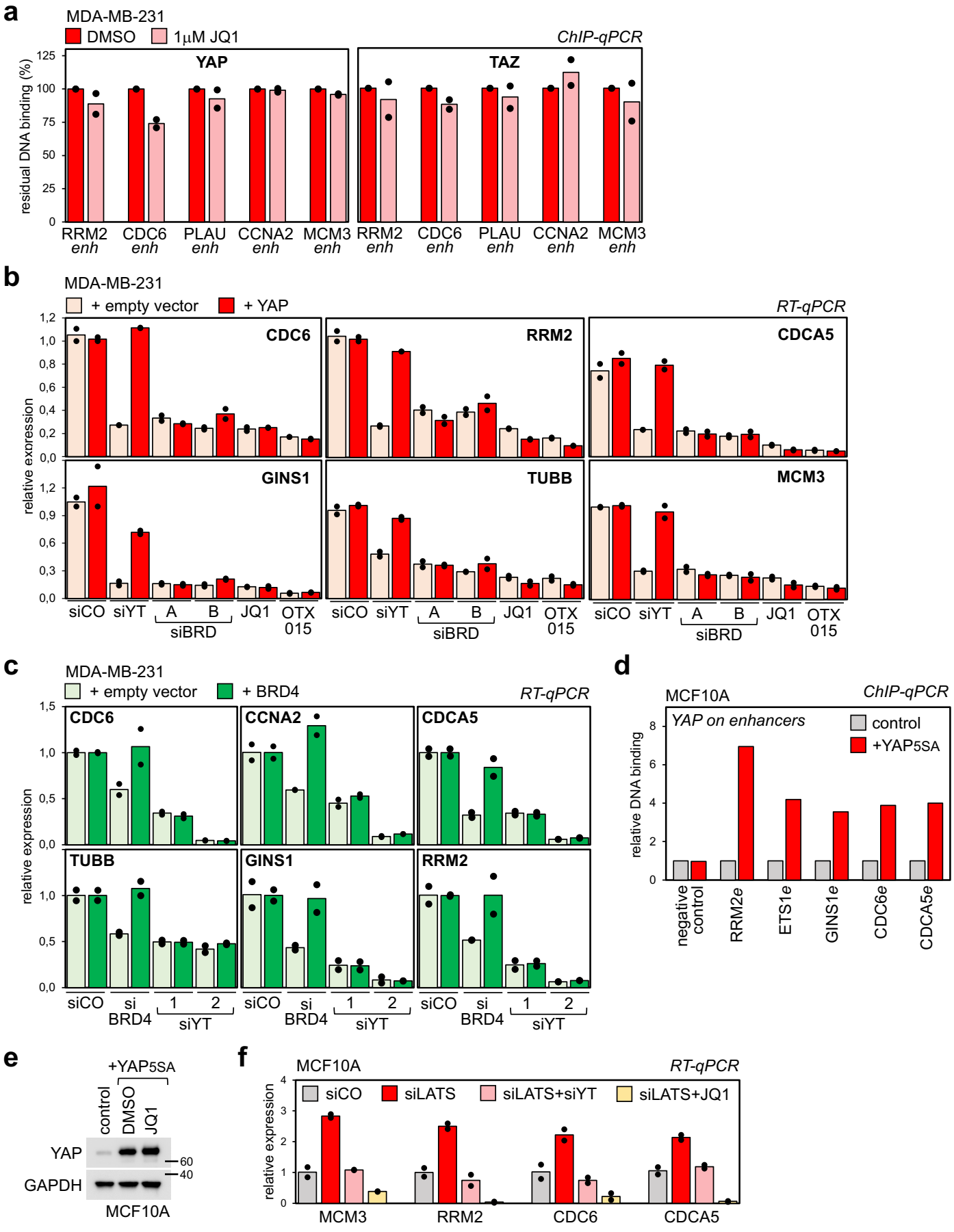

SUPPLEMENTARY FIGURE 4

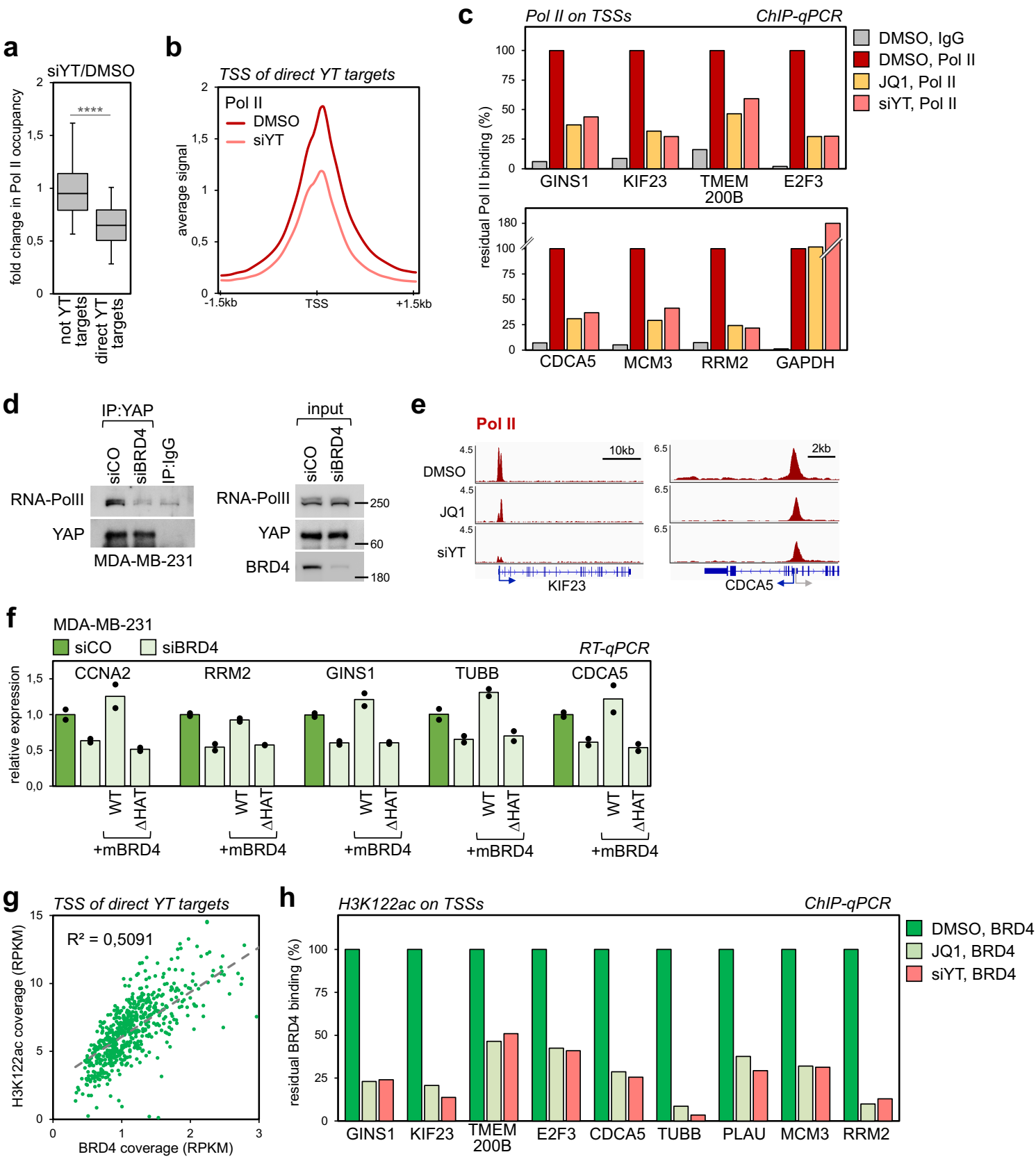

SUPPLEMENTARY FIGURE 5

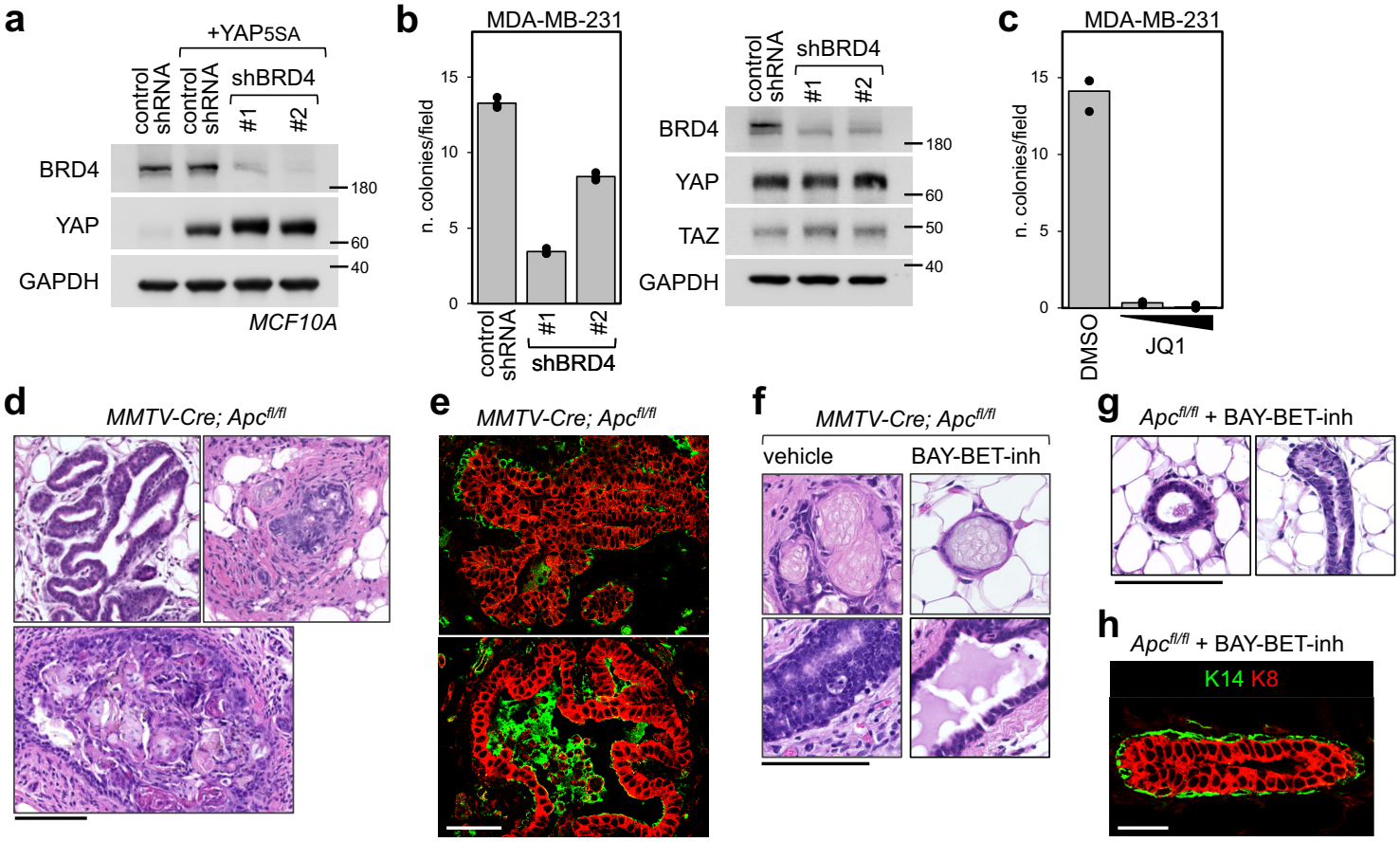

SUPPLEMENTARY FIGURE 6

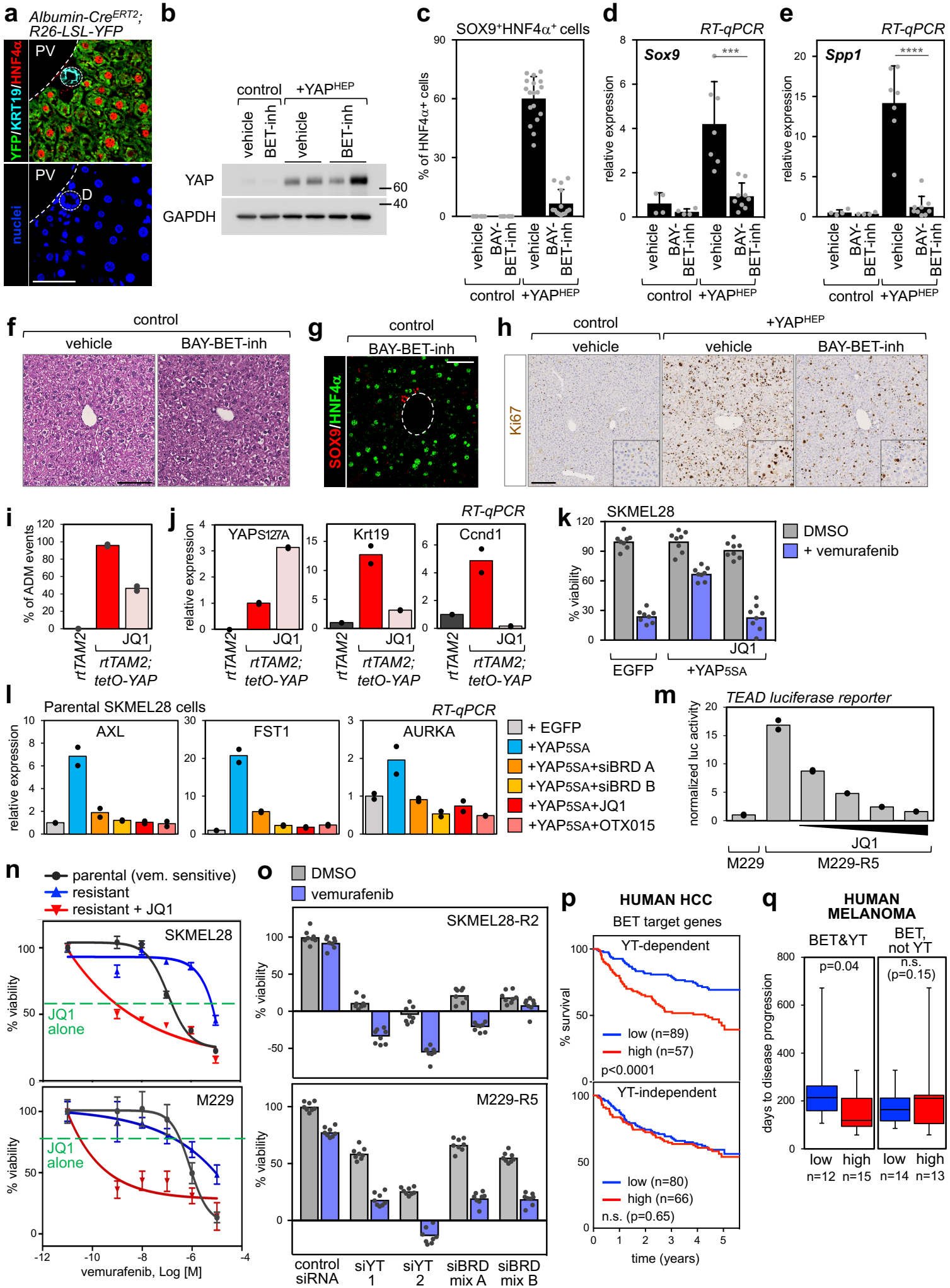

SUPPLEMENTARY FIGURE 7

Figure 1a

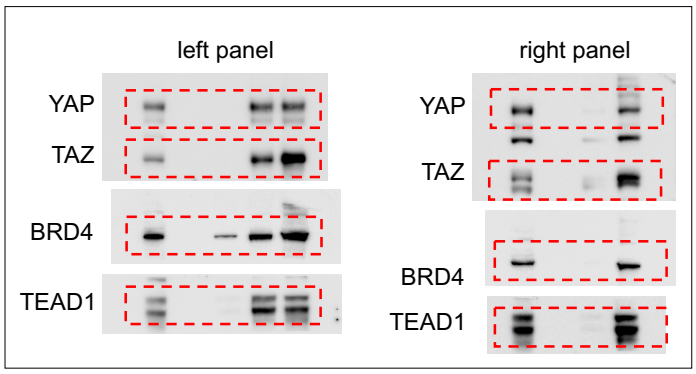

Figure 1c

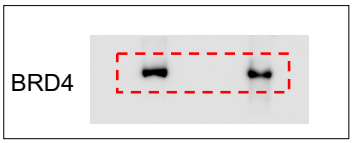

Supplementary figure 1a

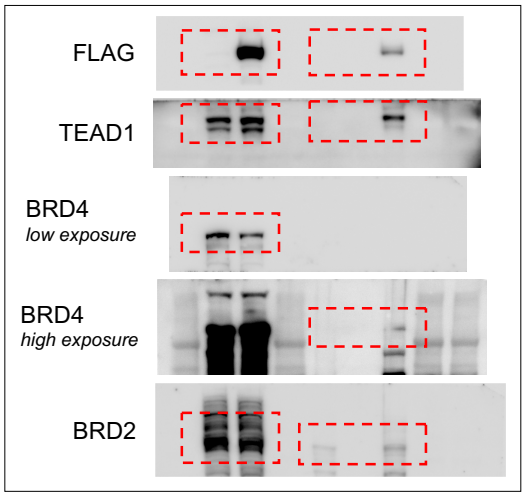

Supplementary figure 1b

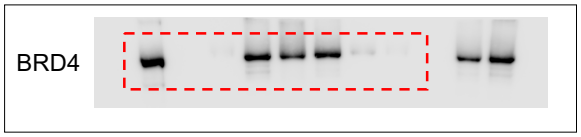

Supplementary figure 1c

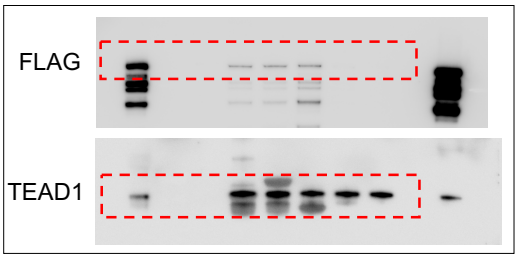

Supplementary figure 1d

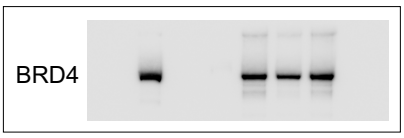

Supplementary figure 2i

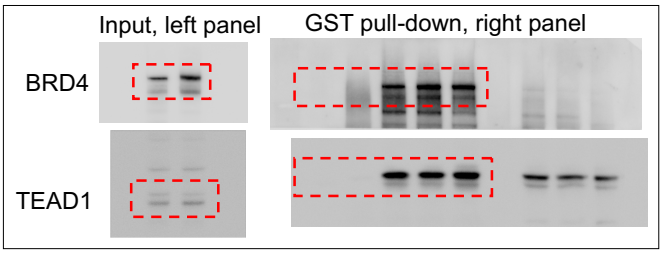

Supplementary figure 3e

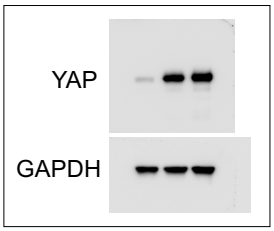

Supplementary figure 4d

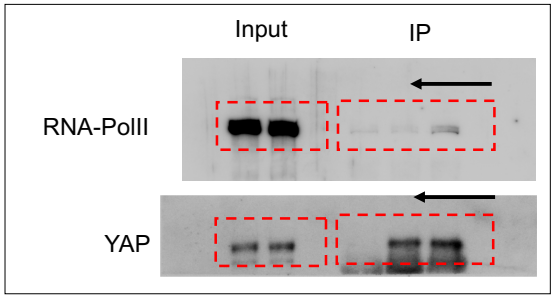

Supplementary figure 5a,b

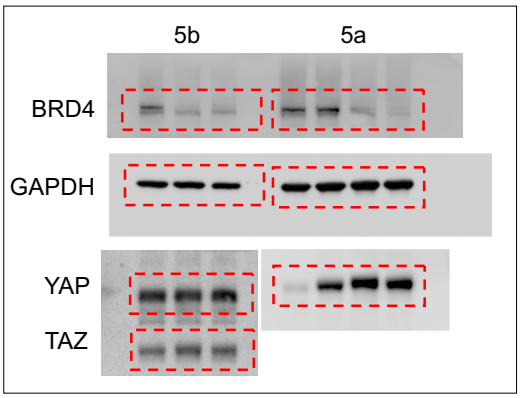

Supplementary figure 6b